Hindawi
Adsorption Science & Technology
Volume 2022, Article ID 9739915, 15 pages
https://doi.org/10.1155/2022/9739915

Research Article

Computational-Based Approaches for Predicting Biochemical Oxygen Demand (BOD) Removal in Adsorption Process

Mohamed K. Mostafa,[1] **Ahmed S. Mahmoud**,[2] **Mohamed S. Mahmoud**,[3] **and Mahmoud Nasr**[4,5]

[1]*Faculty of Engineering and Technology, Badr University in Cairo (BUC), Cairo, Egypt*
[2]*Scientific Research Development Unit, Egyptian Russian University (ERU), Badr, Egypt*
[3]*Sanitary and Environmental Engineering Institute (SEI), Housing and Building National Research Center (HBRC), Egypt*
[4]*Environmental Engineering Department, Egypt-Japan University of Science and Technology (E-JUST), New Borg El-Arab City Alexandria 21934, Egypt*
[5]*Sanitary Engineering Department, Faculty of Engineering, Alexandria University, P.O. Box 21544, Alexandria 21526, Egypt*

Correspondence should be addressed to Mahmoud Nasr; mahmoud.nasr@ejust.edu.eg

Received 8 March 2022; Revised 22 April 2022; Accepted 27 April 2022; Published 10 May 2022

Academic Editor: Stefano Salvestrini

Predicting the adsorption performance to remove organic pollutants from wastewater is an essential environmental-related topic, requiring knowledge of various statistical tools and artificial intelligence techniques. Hence, this study is the first to develop a quadratic regression model and artificial neural network (ANN) for predicting biochemical oxygen demand (BOD) removal under different adsorption conditions. Nanozero-valent iron encapsulated into cellulose acetate (CA/nZVI) was synthesized, characterized by XRD, SEM, and EDS, and used as an efficient adsorbent for BOD reduction. Results indicated that the medium pH and adsorption time should be adjusted around 7 and 30 min, respectively, to maintain the highest BOD removal efficiency of 96.4% at initial BOD concentration $(C_o) = 100$ mg/L, mixing rate = 200 rpm, and adsorbent dosage of 3 g/L. An optimized ANN structure of 5–10–1, with the "*trainlm*" back-propagation learning algorithm, achieved the highest predictive performance for BOD removal (R^2: 0.972, Adj-R^2: 0.971, RMSE: 1.449, and SSE: 56.680). Based on the ANN sensitivity analysis, the relative importance of the adsorption factors could be arranged as pH > adsorbent dosage > time ≈ stirring speed > C_o. A quadratic regression model was developed to visualize the impacts of adsorption factors on the BOD removal efficiency, optimizing pH at 7.3 and time at 46.2 min. The accuracy of the quadratic regression and ANN models in predicting BOD removal was approximately comparable. Hence, these computational-based methods could further maximize the performance of CA/nZVI material for removing BOD from wastewater under different adsorption conditions. The applicability of these modeling techniques would guide the stakeholders and industrial sector to overcome the nonlinearity and complexity issues related to the adsorption process.

1. Introduction

Recently, adsorption has been employed in several types of research as an efficient and reliable process for wastewater treatment [1–3]. The adsorption systems neither consume a lot of electricity nor generate large amounts of sludge [4, 5]. Moreover, the adsorbent material could be appropriately synthesized to provide effective adsorption sites to capture the pollutants from wastewater [6, 7]. However, the adsorption process is highly influenced by several operational factors such as time, pH, and mixing speed [8]. The correlation between these environmental factors and pollutant removal efficiency could be described by nonlinear and complex modeling methods [9]. Hence, more studies are required to investigate the applicability of various statistical tools and artificial intelligence techniques for predicting adsorption performance.

Artificial neural network (ANN) models have been used in recently published studies as a proper method to describe the adsorption performance in relation to operational conditions [10–12]. The architecture of ANN is composed of multiple processing elements (or units) arranged in layers. These units, known as neurons, are highly interconnected and work in parallel to solve complex problems and get relevant relationships among the input attributes. For instance, Mahmoud et al. [13] found that an ANN model could simulate and predict phosphate removal in adsorption experimentation, showing a predictive accuracy of R^2: 0.976. Several operational factors such as solution pH, adsorbent dosage, and mixing speed were used in the adsorption process, showing that pH was the most influential attribute [13]. Hamdy et al. [14] also demonstrated that the removal efficiency of methylene blue (MB) dye from wastewater could be explained by several adsorption factors incorporated into an ANN model (R^2: 0.931). These input attributes included medium pH, initial MB level, and adsorption time; among them, time was the most influential factor [14].

Several researchers have also used regression models and a combination of statistical tools to predict the treatment performance under different operational factors. For example, Fawzy et al. [15] used a quadratic regression model to predict the Ni(II) removal efficiency via adsorption onto plant biomass. The quadratic equation described the correlation between Ni(II) and several inputs (e.g., pH, biomass dosage, and adsorption time) with high predictive accuracy of R^2 = 0.837 [15]. Their study demonstrated that the statistical model could appropriately illustrate the interaction among the input parameters and the shape of the input-output curve [15]. In another study, Fawzy et al. [16] employed a quadratic model to predict the Cd(II) removal efficiency via adsorption onto *Gossypium barbadense* waste. Total Cd(II) removal was achieved under the optimized condition of pH = 7.61, biosorbent diameter = 0.125–0.25 mm, and biosorbent dosage = 24.74 g/L within 109.77 min at initial Cd(II) = 50 mg/L [16].

Given the aforementioned aspects, the application of the computational approaches to describe the adsorption process is an essential point of research. However, further investigations are required to verify the implementation of ANN and quadratic models to predict organic matter removal. This objective would offer a feasible and sustainable approach to domestic wastewater treatment.

Hence, this research focused on predicting and optimizing the BOD removal performance in adsorption experimentation by a computational-based approach (quadratic regression and ANN models). In particular, the study objectives are fourfold: (1) characterization of adsorbent material synthesized by the entrapment of nanozero-valent iron into cellulose acetate polymer (CA-nZVI), i.e., this material has been widely used in the adsorption system due to its proper mechanical strength, thermal stability, and accessibility; (2) use of the CA-nZVI adsorbent to reduce organic matter from wastewater, expressed by BOD, i.e., BOD is considered the standard criterion for assessing the organic pollution of domestic wastewater; (3) describe the influence of various adsorption factors, i.e., pH, adsorbent dosage, time, mixing rate, and initial BOD concentration (C_o), on BOD removal efficiency; and (4) employ computational techniques, i.e., ANN and polynomial regression models, to predict and optimize the adsorption process.

2. Materials and Methods

2.1. Preparation of Adsorbent Material. For preparing an iron solution, around 0.0037 M of ferric chloride hexahydrate ($FeCl_3{\cdot}6H_2O$; 98.5% pure, Arabic lab.) was dissolved in 60 mL of a mixture of 4 (ethanol; C_2H_6O, 95% pure, World Co.) : 1 (deionized water). In parallel, 0.7564 g of reducing sodium borohydride ($NaBH_4$; 99% pure, Win lab.) was dissolved in 200 mL of deionized water to prepare the $NaBH_4$ solution. Further, the reducing $NaBH_4$ solution was placed in a burette and added drop by drop into the prepared iron solution. Black iron nanoparticles precipitate as a result of the direct reaction (Equation ((1)). The iron nanoparticles, known as nZVI, were then washed with distilled water and dried at 75°C for 5 h:

$$2FeCl_3(aq) + 6NaBH_4(aq) + 18H_2O \longrightarrow 2Fe^0(s) + 21H_2(g) + 6B(OH)_3(aq) + 6NaCl(aq). \quad (1)$$

Further, the prepared nZVI was capsulated into cellulose acetate (CA; 99%, Oxford) polymer, using the phase inversion approach [17]. Briefly, at room temperature, 4 g of CA was dissolved in 25 mL dimethylformamide (DMF; 99.99%, Fisher Chemical) solution and then mixed at 300 rpm until complete dissolution (within approximately 60 min). About 0.4 g of nZVI was mixed into the dissolved CA solution for 10 min before being cast into a gelation bath. The preparation of the gelation bath included 2 L of nonsolvent distilled water, 2 wt% DMF, and 0.2 wt% sodium lauryl sulphate (SLS). The prepared CA/nZVI beads (around 3–4 mm in diameter) were collected and washed with distilled water and then used for the adsorption experimentation.

2.2. Preparation of BOD Containing Solution (Adsorbate). Raw wastewater samples were collected from a sewage treatment plant located in New Cairo, Egypt. The samples were analyzed for BOD and subjected to different dilution regimes with ultrapure water. Working stock solutions with BOD concentrations of about 100, 200, 300, 400, and 500 mg/L were prepared and used for the individual experiments.

2.3. Batch Studies on Adsorption. Batch experiments were conducted to determine the effects of adsorption factors on the BOD removal efficiency. For this objective, a one-factor-at-a-time approach was used to prepare the batch assays statistically (Table 1). The factors (pH, CA/nZVI dosage, time, stirring rate, and C_o) and the associated range values were selected following the approaches of previous studies [18–20]. After each experimental run, the percentage of BOD removal (R) and the quantity of sorbed BOD were calculated by Equations (2) and (3). All tests were performed in triplicate, and the average values were recorded:

Table 1: Operating conditions of batch adsorption experiments for BOD removal.

Experimental assay	pH	Dosage (g/L)	Time (min)	Stirring rate (rpm)	C_o (mg/L)
Effect of pH	3–11	3	25	200	300
Effect of adsorbent dose	7	1–5	25	200	300
Effect of contact time	7	3	5–60	200	300
Effect of stirring rate	7	3	25	100–500	300
Effect of BOD concentration	7	3	25	200	100–500

$$R\,(\%) = \left(\frac{C_0 - C_e}{C_0}\right) \times 100, \tag{2}$$

$$q_e\,(\mathrm{mg/g}) = \frac{(C_0 - C_e)V}{M}, \tag{3}$$

where C_o and C_e refer to the initial and equilibrium BOD concentrations (in mg/L), respectively, q_e represents the equilibrium adsorption capacity (mg/g), V is aqueous phase volume (L), and M represents the adsorbent's dry mass (mg).

2.4. Analytical Analysis. The concentrations of BOD in the aqueous solutions were determined using the procedures of *Standard Methods for the Examination of Water and Wastewater* [21]. An X-ray diffractometer (PANalytical's, X'Pert PRO MRD, Netherlands) was used to determine the X-ray diffraction (XRD) patterns of the synthesized nZVI. The XRD equipment was operated with current and voltage levels of 30 mA and 40 kV, respectively. A copper (Cu) K-alpha radiation with a wavelength $(\lambda) = 1.5406$ Å was used to record the XRD patterns in a 40–90° range (step size of 0.02°) [14]. The XRD spectra were used to estimate the crystallite size of the prepared nanoparticles, following Scherrer's formula:

$$D = \frac{K \quad \lambda}{\beta \quad \cos}, \tag{4}$$

where D is the average crystal size, K is the nanoparticle shape factor, θ is the peak diffraction angle, β is pure diffraction broadening, and λ is the X-ray wavelength.

The nanoparticles' surface morphology was measured by a scanning electron microscope (Philips SEM, Quanta 250 field emission gun (FEG), USA). The elemental composition of nZVI was analyzed using energy-dispersive spectroscopy (EDS) in conjunction with SEM at a high magnification of 16kx. For determining the pH at the point of zero charge (pH_{PZC}), the solution pH was incrementally adjusted from 2 to 12 using either 1 N H_2SO_4 or 1 N NaOH (pH_i) in a 100 mL Erlenmeyer flask. About 0.1 g of nZVI was added to the flasks and kept at 23°C for 24 h, and then, the final pH readings were recorded (pH_f).

2.5. Computational-Based Studies

2.5.1. Artificial Intelligence Neural Networks. Figure 1 shows the ANN architecture used to predict BOD removal from a given dataset of five input variables (pH, adsorbent dose, time, stirring rate, and C_o), forming 25 experimental runs. The ANN model is composed of three subsequent layers, i.e., an input layer with 5 neurons, a hidden layer with multiple neurons (m), and the last layer with a single neuron. Each node in the hidden layer is interconnected with a number of weighted signals from the neurons of the 5-length input vector ($P_{5\times1}$). In particular, the inputs were weighted using a $m \times 5$ weight matrix ($W_{m\times5}$) and summed up, giving the formula of $\Sigma W_{m\times5} \cdot P_{5\times1}$. This expression was added to a m-length bias ($b_{m\times1}$), and then, a tangent sigmoid (tansig) transfer function was employed to generate an output; $a_{m\times1} = \mathrm{tansig}(\Sigma W_{m\times5} \cdot P_{5\times1} + b_{m\times1})$. This output was weighted using a $1 \times m$ weight matrix ($W_{1\times m}$), and then, a 1-length bias ($b_{1\times1}$) was added. Finally, a linear (purlin) transfer function was used to generate a single neuron in the output layer using the formula of $a_{1\times1} = \mathrm{purlin}(\Sigma W_{1\times m} \cdot a_{m\times1} + b_{1\times1})$. The "tansig" transfer function limits the output between −1 and +1, whereas the "purlin" function generates outputs in the $-\infty$ to $+\infty$ range [22]. The ANN output was compared with the actual BOD removal efficiencies, and the network weights and biases were adapted until reaching the best predictive performance. The total data describing the inputs-target correlations were randomly separated into three subgroups: training (70%), validation (15%), and testing (15%).

During the ANN learning phase with a back-propagation technique, the weights and biases were adjusted using several epochs (trials). The mean squared error (MSE) between the ANN output and measured BOD removal reached its minimum value at the best network performance. This feed-forward ANN model was used for its simplicity (no cycles or loops) to describe complex input-output relationships and to cope with the weighting adjustment issues [23]. In this study, the number of neurons (m) and the training algorithms were optimized to develop the most suitable ANN architecture. The MATLAB (R2015a) software was used to perform all the ANN computations.

2.5.2. Regression Analysis. A quadratic regression model (Equation (5)) was developed to predict BOD removal and estimate the optimum adsorption condition. Moreover, the results of the polynomial model were used to visualize the correlation between BOD removal and the adsorption factors. The model parameters were estimated based on the least square method [24] to fit the BOD removal data. The goodness-of-fit criteria (R^2 and Adj-R^2) were used to assess the predictive accuracy of the quadratic model [25]. The t-test was used to verify the significance level ($\alpha = 0.05$) among the adsorption variables [26]. The MATLAB (R2015a) software was used to conduct all the statistical calculations:

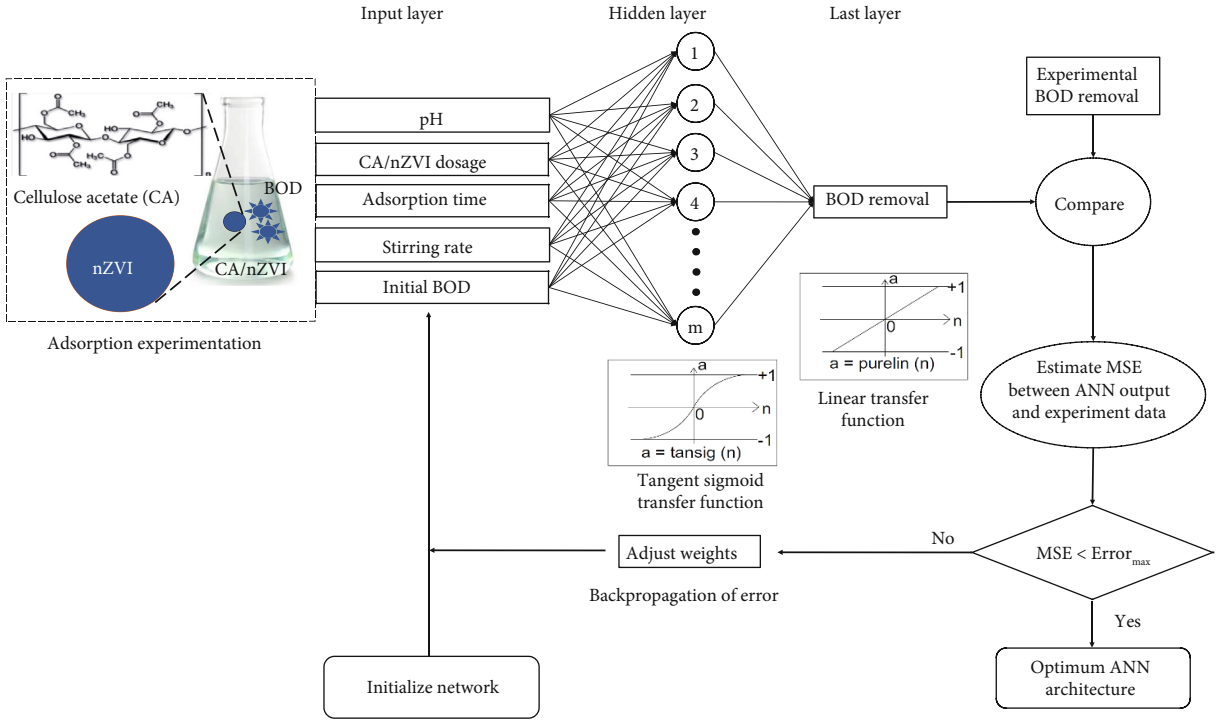

Figure 1: Flowchart of feed-forward back-propagation ANN model for predicting BOD removal efficiency using five adsorption factors, i.e., solution pH, CA/nZVI dosage, time, stirring speed, and initial BOD concentration.

$$Y = \beta_0 + \beta_i(x_i) + \beta_{ii}(x_i)^2, \quad (5)$$

where Y is the BOD removal efficiency predicted using the inputs (x_i), β_0 is the model intercept, and β_i and β_{ii} represent the constants associated with the linear and squared forms of the inputs, respectively.

3. Results and Discussion

3.1. Characterization of nZVI. Figure 2(a) shows the XRD pattern in the 2θ range of 40–90° for the prepared nZVI. Two peaks were recorded at $2\theta \approx 44.6$ and 64.9° for planes Fe (110) and Fe (200), respectively. The results of XRD demonstrated the dominance of zero-valent iron (Fe^0) in the prepared nanoparticles. Comparable XRD peaks related to nZVI characterization have been reported elsewhere [13, 27]. Based on Scherrer's equation, the particle size of the prepared nZVI adsorbent ranged from 23 to 59 nm, obeying the results provided by the SEM morphological study (Figure 2(b)). In particular, the SEM image of the synthesized nZVI showed a heterogeneous and irregular pore structure with particle sizes ranging from 33 to 56 nm. Additionally, many pores were observed in the prepared nanoparticles, facilitating the diffusion and mass transfer of molecules inside the nanomaterial [28]. The SEM image also showed the presence of larger nanoclusters (agglomerated particles), which could be assigned to the magnetic forces existing between the iron nanoparticles. Similar chainlike aggregates and surface tension properties have also been reported while preparing the nZVI material [29]. The EDS analysis observed the presence of iron, gold, and oxygen with an elemental weight content of 51.49%, 34.53%, and 13.98, respectively (Figure 2(c)). The oxygen element could be generated from the oxidation reaction with air and/or water in the outer layer of nZVI. The oxide formation on the nanoparticles' surface layer has also been reported [30]. Moreover, the detection of the Au signal in EDS could assign to the sample coating with a gold layer, following the laboratory analytical procedure [31]. The plot of ΔpH versus pH_i indicated that the pH_{PZC} of nZVI could be determined around 7.5 (Figure 2(d)). At this pH_{PZC}, the net surface charge of nZVI became zero, where the nZVI surface would be positively charged at $pH < pH_{PZC}$ and negatively charged at $pH > pH_{PZC}$ [32]. Moreover, at $pH > pH_{PZC}$, the nZVI particles could partially disaggregate because of surface charge repulsion [33].

3.2. Effect of Operating Conditions on BOD Removal. The BOD removal efficiency varied considerably in response to the change in the adsorption factors (Figure 3). For instance, adapting the solution pH to 7–8 would provide a suitable condition for BOD reduction (Figure 3(a)). This pH range complied with the pH_{PZC}, supporting the involvement of strong attractive and binding forces to remove organic impurities. Moreover, the optimum pH condition would facilitate the generation of hydroxyl radicals (·OH) to degrade and oxidize a series of organic compounds [29]. However, decreasing the pH level below pH_{PZC} was associated with unsatisfactory BOD removal, probably due to the dissolution and/or separation of Fe from nZVI [34]. The BOD removal efficiency was also maximized (above 90%) at pH of 7 in an adsorption process using mixed adsorbent

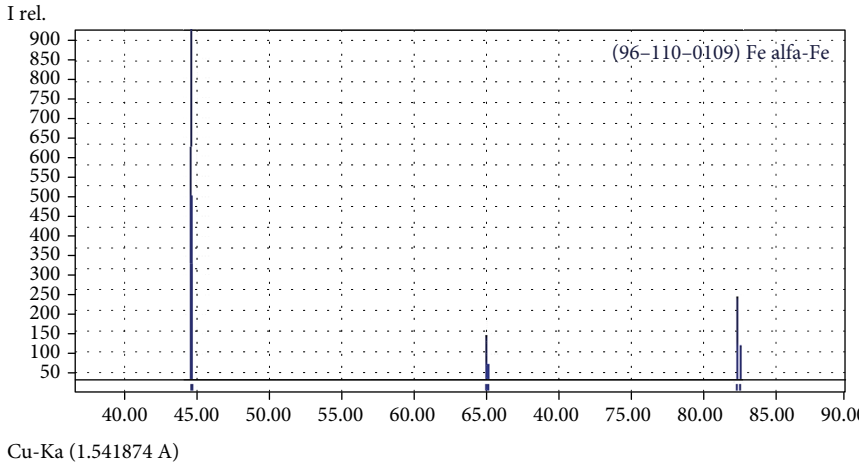

(a)

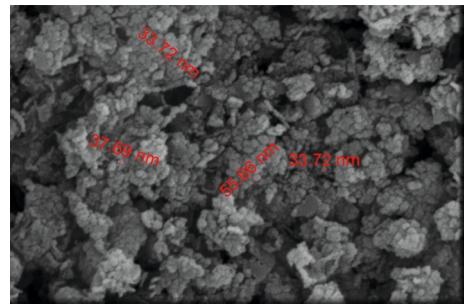

(b)

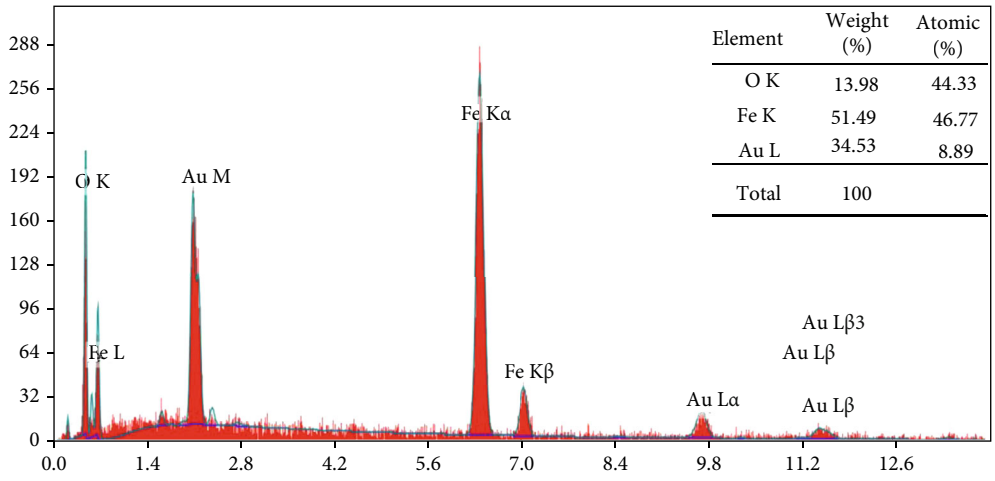

(c)

Figure 2: Continued.

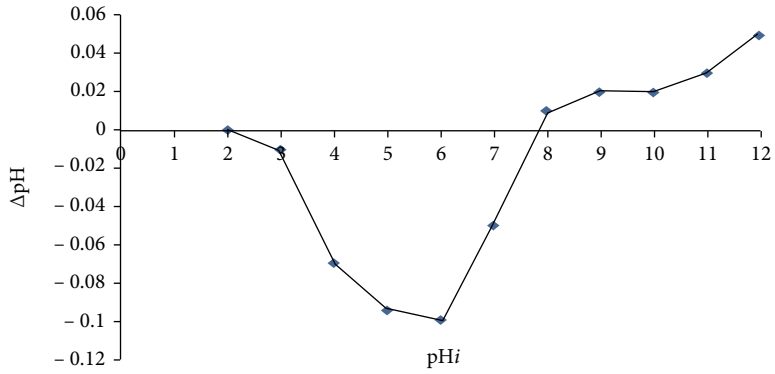

(d)

Figure 2: Characterization of the prepared CA/nZVI adsorbent (a) XRD, (b) SEM, (c) EDS, and (d) pH_{PZC}.

carbon [35]. Their study also demonstrated that the alkaline condition ($pH > pH_{PZC}$) would promote the abundance of OH^- ions to hinder the diffusion of organic ions [35].

The BOD removal efficiency was also enhanced by increasing the CA/nZVI dosage for the 1–5 g/L range (Figure 3(b)). For instance, the BOD removal efficiency improved from 66.3% to 83.2% when the CA/nZVI dosage increased from 1.0 g/L to 5.0 g/L, respectively. Increasing the adsorbent dosage provided more vacant sites to capture large amounts of organic ions. Similar behavior was observed for organic matter removal via an adsorption system with wood fly ash (adsorbent), showing an increase in BOD removal from 4 to 24% with elevating the dosage from 20 to 160 g/L, respectively [36]. Their study demonstrated that raising the adsorbent dosage was accompanied by greater surface area and carbon content, finally promoting higher sorption of organic pollutants [36].

The adsorption time within the range of 5–60 min also influenced the BOD removal efficiency (Figure 3(c)). A high BOD reduction (61.5%) occurred rapidly within the first 10 min, assigning to the availability of a large number of vacant sites at the initial stage. This BOD removal reached 76.8% after 25 min and then slightly increased to 81.2% after 60 min (Figure 3(c)). It could be observed that the adsorption process started to reach the equilibrium state after 25 min due to nZVI saturation. This time was shorter than 60 min used to remove BOD with an efficiency of 91.3% via adsorption onto green synthesized nanomaterials [37].

The BOD removal efficiency also varied according to the rate of mixing nZVI particles in the aqueous solutions (Figure 3(d)). The mixing speed of about 200–300 rpm was suitable to improve BOD removal due to facilitating the transfer and diffusion of organic ions through the nZVI pores. However, increasing the mixing speed over 300 rpm would not be recommended in the adsorption process, probably due to further desorption of the captured contaminants under fast agitation. Moreover, the operational cost of the adsorption system would be expensive due to the surplus electricity input to reach 500 rpm.

The results in Figure 3(e) depict that increasing C_o in the 100–500 mg/L range was associated with a drop in BOD removal from 96.4% to 61.5%. Most vacant adsorption sites are available for entrapping organic ions at low C_o, in agreement with previous results [27, 37, 38]. Increasing C_o tends to provide a driving force to overcome the mass transfer resistance of solute onto nZVI. However, at a high C_o condition, the adsorption capacity of nZVI would suffer from increased competition among organic ions and blockage of the available active sites [10]. This finding verifies the slight reduction in the adsorption performance at an excessive C_o.

3.3. BOD Removal by Different Adsorbents Reported in the Literature. Table 2 includes the removal efficiencies of BOD using various adsorbent materials reported in the literature compared to CA/nZVI applied in this study. For example, Mahmoud et al. [37] used soft black tea to prepare nZVI, which removed 91.3% of BOD at pH 8, stirring rate 200 rpm, and adsorbent dosage 3.2 g/L within 60 min. To avoid the unmanaged disposal of wood residues, Laohaprapanon et al. [36] used wood fly ash to remove BOD via batch sorption experiments. Their study achieved BOD removal of 24% using an ash dosage of 160 g/L within 20 min. Due to its high carbon content and quite accessibility, date palm waste was used to prepare activated carbon, which is further employed for organic matter adsorption [39]. Their study showed that 1 g/L of this activated carbon could eliminate 92.8% of BOD at pH = 6.0, agitation rate = 400 rpm, and 25°C within 150 min [39]. It could be noticed that nZVI exhibited higher BOD reduction than the application of agricultural wastes. This finding could be assigned to the dual effects of adsorption and degradation caused by nZVI.

3.4. Isotherm and Kinetic Studies. Three isotherm models were used to describe the adsorption equilibrium between organic pollutants and CA/nZVI (Figure 4(a)). These models were Langmuir [40] (Equation (6)), Freundlich [41] (Equation (7)), and Tempkin and Pyzhev [42] (Equation (8)):

$$\frac{C_e}{q_e} = \left(\frac{1}{Q_m}\right) C_e + \frac{1}{K_L \cdot Q_m}, \quad (6)$$

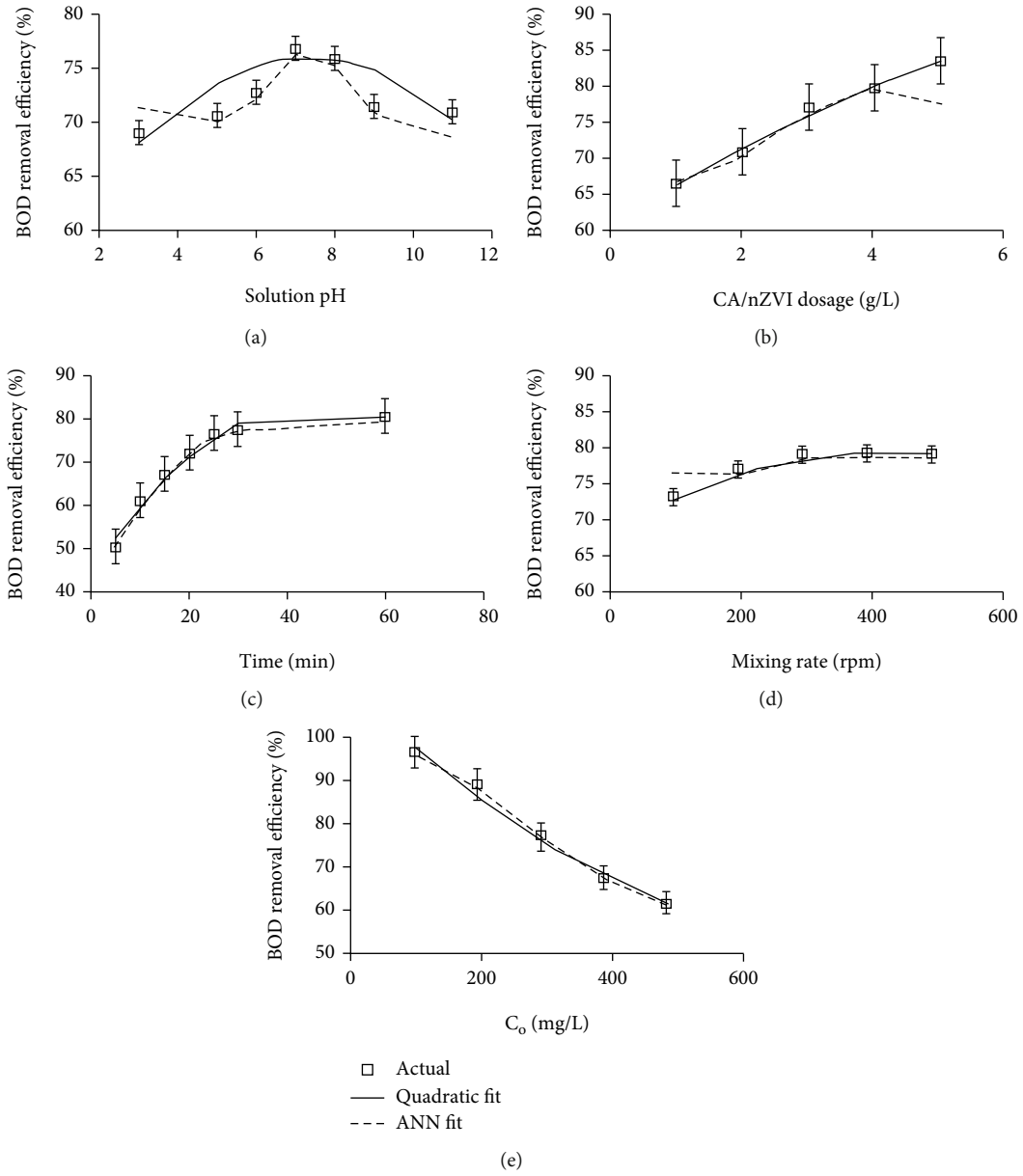

Figure 3: Influences of adsorption factors on BOD removal efficiency: (a) solution pH, (b) adsorbent dosage, (c) contact time, (d) stirring rate, and (e) initial adsorbate concentration.

$$\log(q_e) = \left(\frac{1}{n}\right) \log(C_e) + \log(K_F), \quad (7)$$

$$q_e = B_T \ln(A_T) + B_T \ln(C_e), \quad (8)$$

where q_e is the number of biological pollutants adsorbed in the form of BOD at equilibrium per gram of CA/nZVI (mg/g) corresponding to the equilibrium BOD concentration (C_e, in mg/L), Q_m (mg/g), and K_L (L/mg) which are the Langmuir model parameters, $1/n$ and K_F ((mg/g) $(\text{L/mg})^{1/n}$) are the Freundlich model parameters, and B_T (J/mol) and A_T (L/g) are the Tempkin and Pyzhev model parameters.

Table 3 lists the values of isotherm parameters and the corresponding fitting accuracies (R^2 values). A low R^2 of 0.881 obtained by fitting the adsorption data to the Langmuir model suggested that BOD removal by nZVI could not follow the monolayer adsorption hypothesis [43]. The Freundlich model achieved a sufficient fitting accuracy ($R^2 = 0.994$) to describe the adsorption isotherm. This goodness-of-fit indicates that multilayer adsorption and heterogeneous sites could facilitate BOD removal by CA/nZVI [44]. The $1/n$ and K_F values were 0.285 and 23.014 (mg/g) $(\text{L/mg})^{1/n}$, indicating that the adsorption of organic ions onto CA/nZVI was preferable under the experimental conditions. A high R^2 value (0.985) was also observed using

Table 2: Removal efficiencies of BOD using various adsorbent materials reported in literature.

Adsorbent	Experimental factor					Removal efficiency (%)	Reference
	Adsorbent dosage (g/L)	pH	C_o (mg/L)	Time (min)	Stirring rate (rpm)		
Wood fly ash	160	1.4	15001	20	600	24	Laohaprapanon et al. [36]
$FeSO_4{\cdot}7H_2O$ coagulant	2.0	5	25500	30	200/50	78	Hossain et al. [46]
nZVI from black tea extract	3.2	8.0	365	60	200	91.3	Mahmoud et al. [37]
Activated carbon prepared from date palm waste	1.0	6.0	14	150	400	92.8	Nayl et al. [39]
CA/nZVI	3.0	7.0	100	30	200	96.4	This study
Mixed adsorbent carbon	35	7	505	150	600	99.1	Devi and Dahiya [35]
Commercial activated carbon	40	2	505	180	600	99.5	Devi and Dahiya [35]

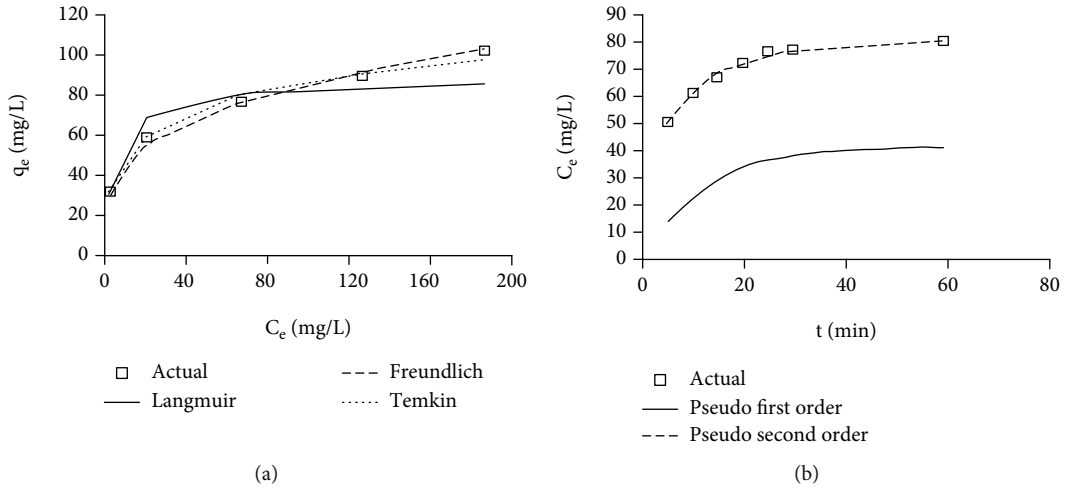

Figure 4: Fitting of adsorption data to (a) isotherm models and (b) kinetic models.

Table 3: Results of isotherm and kinetic studies for BOD removal by CA/nZVI adsorbent.

Model	Parameter	Fitting formula	Fitting accuracy (R^2)
Langmuir isotherm	$Q_m = 88.496$ mg/g $K_L = 0.155$ L/mg $R_L = 0.013$–0.060	$Q_e = 13.755C_e/(1 + 0.155C_e)$	0.881
Freundlich isotherm	$1/n = 0.285$ $K_F = 23.014$ (mg/g) (L/mg)$^{1/n}$	$Q_e = 23.014C_e^{0.285}$	0.994
Tempkin and Pyzhev isotherm	$B_T = 17.009$ J/mol $A_T = 1.630$ L/g	$Q_e = 17.009\ln(1.630C_e)$	0.985
Pseudo-first-order kinetic	$Q_e = 42.442$ mg/g $k_1 = 0.0791$/min	$Q_t = 42.442[1 - \exp(-0.079t)]$	0.997
Pseudo-second-order kinetic	$Q_e = 86.207$ mg/g $k_2 = 0.003$ g/mg/min	$Q_t = 23.202t/(1 + 0.269t)$	0.984

Table 4: Determining the best ANN predictive performance by adapting the number of hidden layer neurons and the back-propagation learning algorithm.

ANN structure	Back-propagation learning algorithm	Coefficient of determination (R^2)			Goodness of fit			
		Training	Validation	Testing	R^2	Adj-R^2	RMSE	SSE
5–3–1	*trainlm*	0.992	0.579	0.931	0.740	0.730	3.067	254.000
5–5–1	*trainlm*	0.174	0.980	0.830	0.198	0.168	3.088	257.500
5–8–1	*trainlm*	0.908	0.955	0.910	0.914	0.911	2.207	131.500
5–10–1	*trainlm*	0.975	0.926	0.998	0.972	0.971	1.449	56.680
5–15–1	*trainlm*	0.752	0.430	0.819	0.741	0.731	4.103	454.500
5–20–1	*trainlm*	0.992	0.994	0.684	0.910	0.908	2.831	216.400
5–10–1	*trainbfg*	0.960	0.992	0.924	0.960	0.949	1.729	80.690
5–10–1	*traingdm*	0.228	0.598	0.399	0.246	0.218	2.359	150.200
5–10–1	*traingda*	0.823	0.740	0.968	0.824	0.819	3.175	272.300
5–10–1	*traincgb*	0.169	0.441	0.027	0.127	0.095	10.940	3234.000
5–10–1	*traincgf*	0.835	0.918	0.507	0.815	0.809	3.762	382.100
5–10–1	*trainoss*	0.904	0.891	0.982	0.906	0.903	2.696	196.200
5–10–1	*trainscg*	0.000	0.005	0.264	0.000	-0.037	10.290	2860.000

the Tempkin and Pyzhevisotherm model, signifying a good fit with the experimental data. The estimated Tempkin and Pyzhev parameters ($B_T = 17.009$ J/mol ; $A_T = 1.630$ L/g) were assigned to the occurrence of physical adsorption and uniform distribution of bounding energies for BOD removal.

The pseudo-first-order (PFO) (Equation (9)) and pseudo-second-order (PSO) (Equation (10))) kinetic models [45] were used to quantitatively describe the kinetic adsorption of organic impurities onto CA/nZVI:

$$\log(q_e - q_t) = \log(q_e) - \frac{k_1}{2.303}t, \tag{9}$$

$$\frac{t}{q_t} = \frac{1}{k_2 \times q_e^2} + \frac{1}{q_e}t, \tag{10}$$

where k_1 (1/min) and k_2 (g/mg/min) are the PFO and PSO constants, respectively, and q_t (mg/g) and q_e (mg/g) represent the amount of adsorbed molecules at time t and equilibrium, respectively.

The plot of q_e vs. t shows the applicability of the adsorption kinetic models for fitting the experimental data (Figure 4(b)). This fitting reveals that the interaction between organic pollutants and CA/nZVI for BOD removal is influenced by the physisorption and chemisorption pathways. In another kinetic adsorption study [39], a chemisorption reaction was dominant for removing BOD by activated carbon. Hossain et al. [46] also demonstrated that the removal of BOD from palm oil mill effluent by coagulation/adsorption using $FeSO_4{\cdot}7H_2O$ followed the PSO kinetic modeling.

3.5. Artificial Neural Network (ANN) for Adsorption Computation

3.5.1. ANN Optimization. Table 4 lists the predictive performances of several ANN structures derived by altering the number of hidden layer neurons and the back-propagation learning algorithm. The input layer (with 5 neurons) received data from the five adsorption factors. Only one hidden layer was used in these ANNs to avoid an overcomplex network's architecture and obey the optimality criterion (e.g., save computational cost, minimize MSE, and fasten the learning speed). The output layer included a single node, and hence, the ANN configuration could be expressed as 5 – m – 1. The network performance was unsatisfactory for small m, probably due to a lower learning capability caused by the insufficient computational neurons. It was also found that 10 neurons yielded the highest R^2 values, where a further increase in the number of neurons would cause more fitted functions and prolong the computation time. Hence, local minima or overfitting might affect the ANN training process by either elevating or lowering the number (m) beyond 10 neurons, finally leading to an imprecise fit. Moreover, Levenberg-Marquardt (*trainlm*) yielded the best goodness-of-fit statistics compared with other learning algorithms. The "*trainlm*" training function is one of the fastest back-propagation algorithms to adapt the weight and bias values [22]. Although some functions such as "*trainbfg*" showed high R^2 values for the training dataset, R^2 of the validation and testing procedures were unsatisfactory. Accordingly, the "*trainlm*" training function with $m = 10$ neurons was selected for the optimized network configuration.

3.5.2. ANN Training, Validation, and Test. During network optimization, the predictive accuracies for the training, validation, and testing processes were recorded (Figure 5(a)). In these figures, the theoretical and best regression fittings are given by the dashed and solid lines, respectively. These processes showed R^2 values of 0.975, 0.926, and 0.998 for the optimum ANN structure (5–10–1), respectively. The overall R^2 value was 0.972, in which the ANN model would explain 97.2% of variability within the BOD removal efficiencies via a linear regression model. Figure 5(b) shows the validation checks during training that stopped at epoch number 6. This epoch corresponded to a validation check of 6, in which the

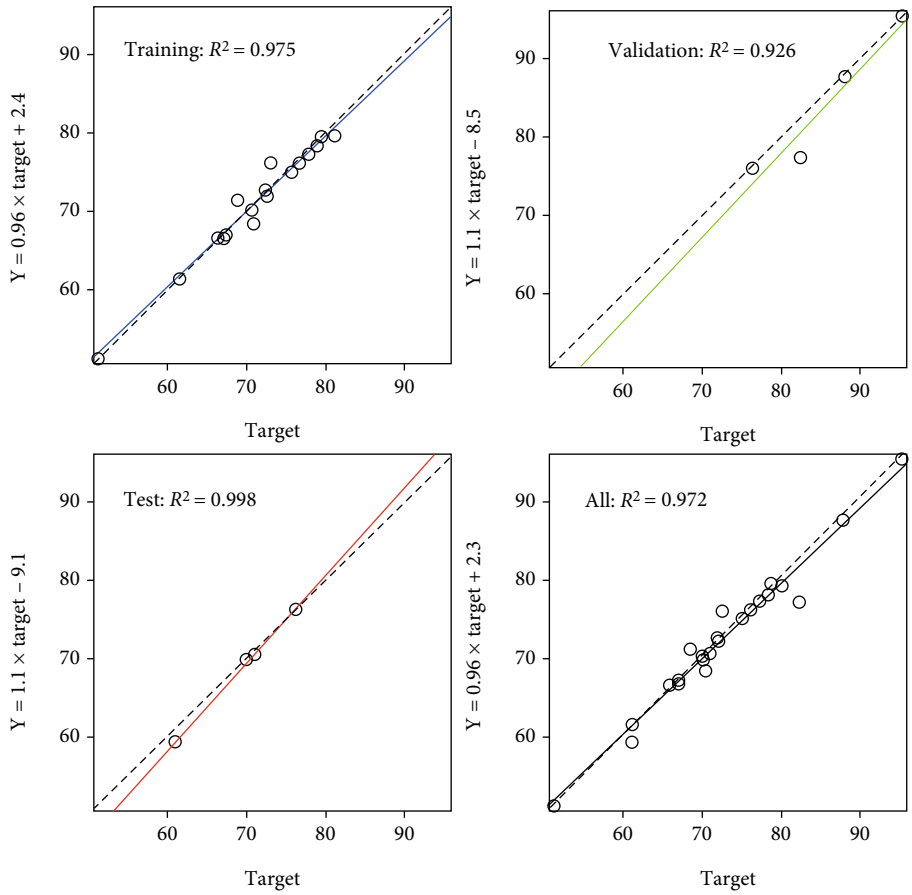

(a)

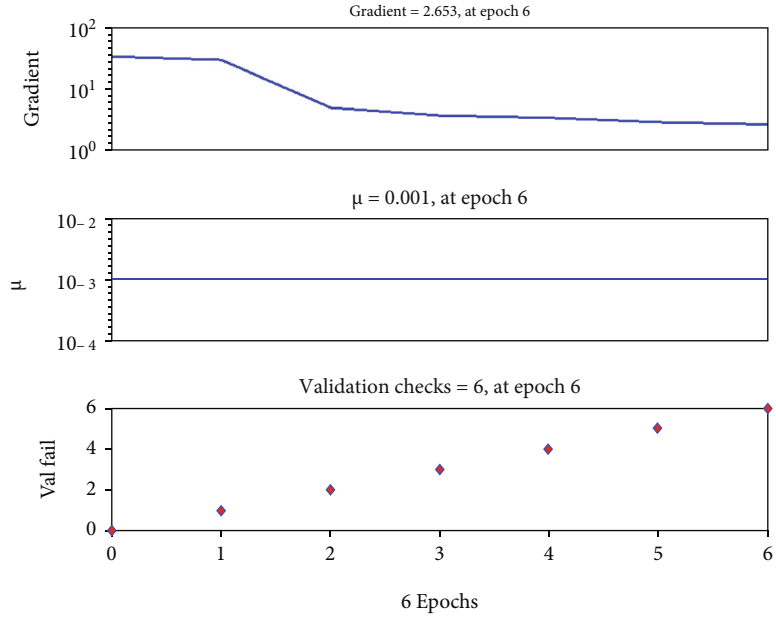

(b)

Figure 5: Continued.

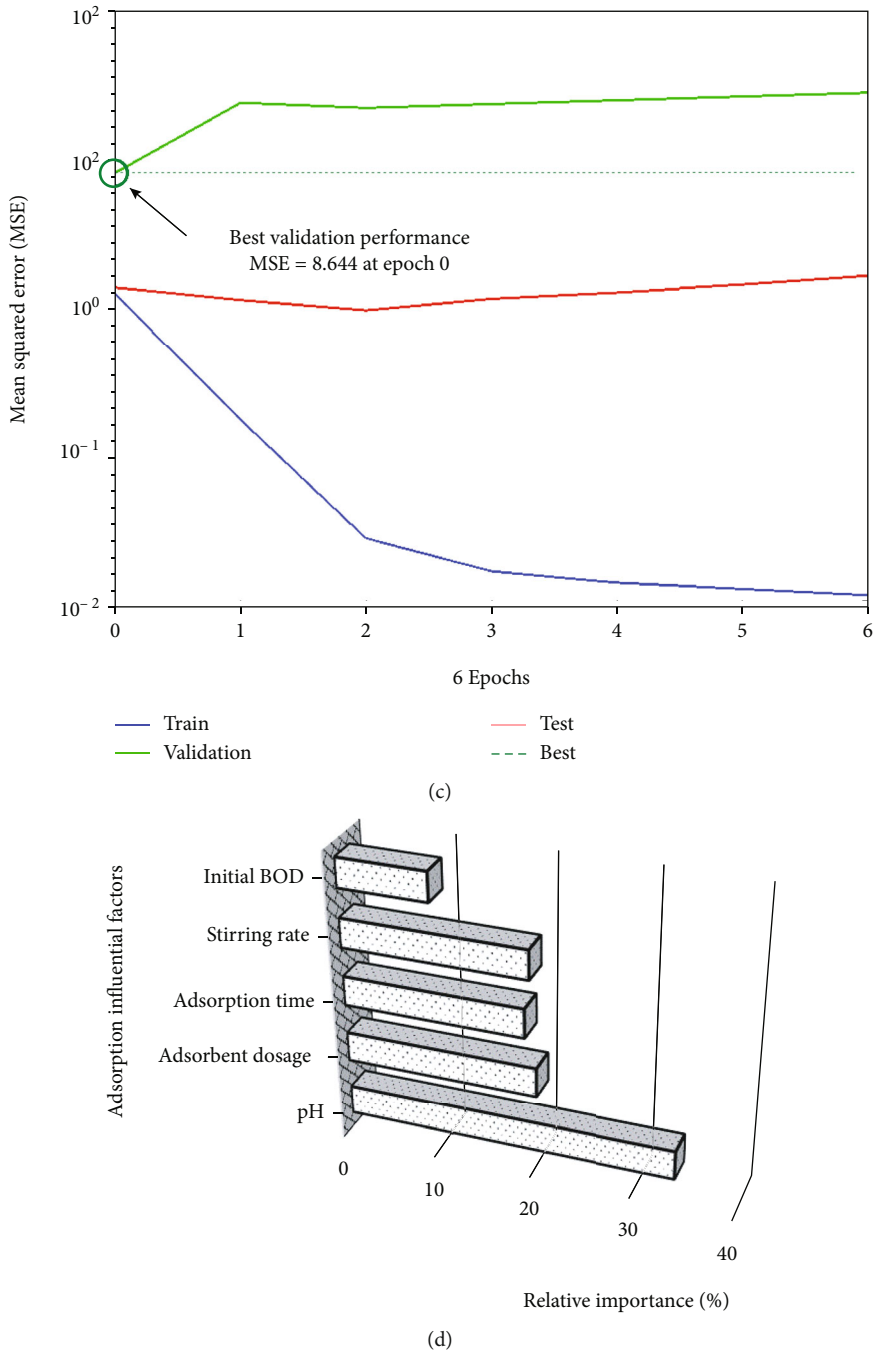

Figure 5: Performance of ANN model for predicting BOD removal efficiency: (a) regression plot, (b) validation checks, (c) best validation, and (d) relative importance. The number of data points in the training, cross-validating, and testing sets had 70%, 15%, and 15% proportions, respectively.

errors were repeated six times before the process termination. During the 6 error repetitions (Figure 5(c)), the MSE of the training dataset dropped due to the fact that "*trainlm*" is an efficient algorithm to improve the learning of ANN subjected to complex relationships [47]. For instance, the ANN parameters (weights and biases) were appropriately adjusted during training. The validation curve initiated to rise after epoch 0, giving the best validation performance at the minimum MSE of 8.644. Based on the validation plot, the ANN model would overfit the data after epoch 0, giving unsatisfactory generalization power. The testing curve gradually declined until epoch 2, followed by a slight rise; where the MSE between the predicted and target outputs increased. The MSE of the testing dataset implied that the ANN model could predict BOD removal using new input records not seen during training and validation. Based on the network performance during training, validation, and test, the optimum weights and biases were determined at epoch 0 to give precise results when importing new input data.

Table 5: t statistics and p values for coefficients of the quadratic regression model to predict BOD removal efficiency. Significant level at $p < 0.05$. Goodness-of-fit indices are $R^2 = 0.973$ and Adj-$R^2 = 0.959$, with MSE = 3.096 and DFE = 18.

Variable	Beta	SE	t ratio	Prob > $\lvert t \rvert$	Effect
Constant	β_0: 33.0635	9.049	3.654	0.002	Significant
pH	β_1: 6.2763	1.202	5.222	0.000	Significant
Dosage	β_2: 6.2479	2.070	3.019	0.007	Significant
Time	β_3: 1.7217	0.123	14.022	0.000	Significant
Rate	β_4: 0.0496	0.027	1.805	0.088	Insignificant
C_o	β_5: -0.1421	0.021	-6.866	0.000	Significant
pH × pH	β_{11}: -0.4274	0.084	-5.110	0.000	Significant
Dosage × dosage	β_{22}: -0.3297	0.332	-0.992	0.334	Insignificant
Time × time	β_{33}: -0.0186	0.002	-10.551	0.000	Significant
Mixing × mixing	β_{44}: -0.0001	0.000	-1.286	0.215	Insignificant
$C_o \times C_o$	β_{55}: 0.0001	0.000	2.549	0.020	Significant

3.5.3. ANN Applicability for Adsorption Studies. In this study, a three-layer feed-forward back-propagation ANN with a "*trainlm*" training algorithm and 5–10–1 architecture was the optimized artificial intelligence model. This model would be beneficial in predicting the adsorption performance to remove BOD under varying environmental conditions. Moreover, the obtained weights ($W_{10\times5}$ and $W_{1\times10}$) and thresholds ($b_{10\times1}$ and $b_{1\times1}$) would be used to determine the relative importance of the input factors. This step was achieved by partitioning the network's connection weights, as reported elsewhere [47, 48].

Figure 5(d) shows each experimental factor's relative importance, where the solution pH experienced the most influence on the BOD removal efficiency. Accordingly, the medium pH should be adjusted to around 7.5 for maintaining the highest adsorption performance. Controlling and adjusting the medium pH would be essentially considered to design and scale up the adsorption system. The relative importance of adsorbent dosage, time, and mixing speed was almost comparable at around 18%. Lower relative importance for C_o could be assigned to the efficient adsorption process for the investigated range of BOD (100–500 mg/L). Moreover, all the relative importance percentages were satisfactory, implying that no input factor could be excluded during the adsorption experimentation.

3.6. Quadratic Regression Model for Adsorption Computation. Table 5 lists the statistical results generalized from the t-test analysis for predicting BOD removal (response variable). The model's performance showed a reliable goodness-of-fit with R^2 of 0.973 and Adj-R^2 of 0.959. Adj-R^2 was approximately comparable to R^2, which could be assigned to the importance of the selected parameters in describing the adsorption process. Moreover, significant ($p < 0.05$) results were observed for the linear correlations of x_1, x_2, x_3, and x_5, suggesting that the BOD removal efficiency would be improved with incrementing pH, dosage, and time. Moreover, an increase in C_o tended to reduce the BOD removal significantly ($p < 0.05$) because the vacant adsorbent sites would be exhausted by increasing the BOD concentration. The model output also showed significant correlations with the quadratic forms of x_1, x_3, and x_5. Hence, a quadratic linear concave up curve would be visualized for the plot of BOD removal against each pH and time. This curve indicated that the improvement of BOD removal after certain values of pH and time would be insignificant ($p > 0.05$). The optimum values of these parameters were numerically assigned as 7.3 and 46.2 min, respectively. Moreover, a quadratic linear convex down shape would be noticed for the plot of BOD removal versus C_o because increasing the BOD concentration would deteriorate the adsorption performance of CA/nZVI. The plot of the BOD removal vs. mixing rate showed a "flat" curve, assigning to the insignificant ($p > 0.05$) influence of the input "x_4" on the model response. This "flat" pattern could be attributed to the narrow range of stirring rate during the investigation, making it imprecise to demonstrate a considerable relationship. Accordingly, the mixing rate was selected as 100 rpm to reduce the cost of the adsorption process.

3.7. Model Verification. The accuracy of the developed computational models to predict BOD removal under new conditions was estimated. In particular, additional 25 experimental runs were performed by varying the adsorption factors, followed by the analysis of BOD concentrations. In parallel, these inputs were incorporated into the quadratic and ANN models to predict the corresponding BOD removal efficiencies. The average of the absolute differences between the experimental results and model outputs was used to estimate the mean absolute error (MAE). The results in Table 6 demonstrate that the MAE values for the ANN and quadratic regression models were 0.73% and 1.91%, respectively. Apparently, both models showed a promising ability to predict the BOD removal efficiencies remarkably close to experimental values. However, the ANN model was more reliable and robust than the quadratic regression method in providing the predictions closer to the measured data. Each of the modeling techniques has advantages, regarding the prediction, optimization, and recognition applications in wastewater treatment processes.

Table 6: Verification of quadratic regression and ANN models for predicting BOD removal using additional experimental runs.

Run	Experimental parameters*					BOD removal efficiency (%)			Absolute error (%)	
	x_1	x_2	x_3	x_4	x_5	Actual	ANN	Quadratic regression model	ANN	Quadratic regression model
1	3	3	25	200	300	69.0	69.0	67.5	0.0	1.5
2	5	3	25	200	300	70.6	70.6	73.2	0.0	2.6
3	6	3	25	200	300	72.7	75.4	74.8	2.7	2.1
4	7	3	25	200	300	76.8	76.8	75.5	0.0	1.3
5	8	3	25	200	300	75.8	74.4	75.4	1.4	0.4
6	9	3	25	200	300	71.4	71.4	74.4	0.0	3.0
7	11	3	25	200	300	70.9	70.9	69.9	0.0	1.0
8	7	1	25	200	300	66.3	66.3	65.7	0.0	0.6
9	7	2	25	200	300	70.5	70.5	70.9	0.0	0.4
10	7	4	25	200	300	79.4	79.4	79.5	0.0	0.1
11	7	5	25	200	300	83.2	83.2	82.8	0.0	0.4
12	7	3	5	200	300	50.7	54.5	52.3	3.8	1.6
13	7	3	10	200	300	61.5	61.5	59.5	0.0	2.0
14	7	3	15	200	300	67.3	67.3	65.8	0.0	1.5
15	7	3	20	200	300	72.4	72.2	71.1	0.2	1.3
16	7	3	30	200	300	77.9	81.0	79.0	3.1	1.1
17	7	3	60	200	300	81.0	81.0	80.5	0.0	0.5
18	7	3	25	100	300	73.0	73.0	73.6	0.0	0.6
19	7	3	25	300	300	78.9	78.9	75.5	0.0	3.4
20	7	3	25	400	300	79.1	79.1	73.5	0.0	5.6
21	7	3	25	500	300	79.0	76.7	69.4	2.3	9.6
22	7	3	25	200	100	96.4	96.4	96.0	0.0	0.4
23	7	3	25	200	200	88.9	93.2	84.7	4.3	4.2
24	7	3	25	200	400	67.4	66.9	68.3	0.5	0.9
25	7	3	25	200	500	61.5	61.5	63.1	0.0	1.6
Mean absolute error (MAE) (%)									0.73	1.91

*x_1 is pH; x_2 is adsorbent dose (g/L); x_3 is contact time (min); x_4 is stirring rate (rpm); x_5 is initial concentration (mg/L).

However, ANN is able to overcome some shortages that could arise during regression analysis implementation. In particular, the input factors do not require a statistical experimental design to train the ANN model (compared to the regression analysis that only provides first- or second-order polynomial models). ANN as a soft computing technique and a black-box model depends on the analysis of available data to simulate any form of nonlinearity. In parallel, the regression models utilize a small number of experiments to generate manifold information, provide graphical illustrations for input-output relationships, and establish significance analysis. Hence, the authorities are encouraged to develop and scale up these modeling approaches in real-scale wastewater adsorption systems.

4. Conclusions

This study focused on the application of computational-based techniques to predict BOD removal in an adsorption process. The adsorbent material was characterized by XRD, SEM, and EDS, showing a successful preparation of Fe nanoparticles in the zero-valent state. The highest BOD removal efficiency (96.4%) was observed at pH = 7, adsorbent dosage = 3 g/L, mixing rate = 200 rpm, and C_o = 100 mg/L within 25 min. A quadratic regression model was developed to enhance BOD reduction, showing optimum pH of 7.3 and time of 46.2 min, equivalent to a BOD removal efficiency of over 99%. Moreover, an ANN structure was properly optimized as 5–10–1 with the "*trainlm*" back-propagation learning algorithm to predict BOD removal (R^2: 0.972, Adj-R^2: 0.971). The results of the computational-based studies revealed that the adjustment of medium pH at the 7–8 range would be essentially considered to design and scale up the adsorption system. The results also showed that the ANN model (MAE 0.73%) was more reliable than the quadratic regression model (MAE 1.91%) in predicting the BOD removal efficiency; however, both models maintained acceptable predictive accuracies. Hence, both modeling approaches would be employed to guide the stakeholders and industrial sector to overcome the nonlinearity and complexity issues associated with the adsorption process. Further studies are required to apply these ANN and quadratic models to enhance organic pollution reduction at a large scale.

Nomenclature

ANN: Artificial neural network
BOD: Biochemical oxygen demand
CA: Cellulose acetate
CA/nZVI: Nanozero-valent iron encapsulated into cellulose acetate
DMF: Dimethylformamide
EDS: Energy-dispersive spectroscopy
$FeCl_3 \cdot 6H_2O$: Ferric chloride hexahydrate
MAE: Mean absolute error
MSE: Mean squared error
$NaBH_4$: Sodium borohydride
PFO: Pseudo-first-order
PSO: Pseudo-second-order
SEM: Scanning electron microscope
SLS: Sodium lauryl sulphate
XRD: X-ray diffraction.

Data Availability

The article includes all data generated or analyzed during the investigation.

Conflicts of Interest

No known competing financial interests or personal relationships could have appeared to influence the study.

Authors' Contributions

All authors contributed to conceptualization, methodology, formal analysis, and writing—review and editing.

Acknowledgments

The authors would like to thank Badr University in Cairo (BUC), Egyptian Russian University (ERU), and Housing and Building National Research Center (HBRC) for supporting this research. The last author acknowledges Nasr Academy for Sustainable Environment (NASE). This work was supported by The Academy of Scientific Research and Technology (ASRT)/the Bibliotheca Alexandrina (BA) Research Grants (grant number 1469) awarded to the first author of this paper (Associate Professor Mohamed K. Mostafa, BUC).

References

[1] Z. Berizi, S. Y. Hashemi, M. Hadi, A. Azari, and A. H. Mahvi, "The study of non-linear kinetics and adsorption isotherm models for Acid Red 18 from aqueous solutions by magnetite nanoparticles and magnetite nanoparticles modified by sodium alginate," *Water Science and Technology*, vol. 74, no. 5, pp. 1235–1242, 2016.

[2] E. Ahmadi, B. Kakavandi, A. Azari et al., "The performance of mesoporous magnetite zeolite nanocomposite in removing dimethyl phthalate from aquatic environments," *Desalination and Water Treatment*, vol. 57, no. 57, pp. 1–15, 2016.

[3] A. G. Kumi, M. G. Ibrahim, M. Fujii, and M. Nasr, "Synthesis of sludge-derived biochar modified with eggshell waste for monoethylene glycol removal from aqueous solutions," *SN Applied Sciences*, vol. 2, no. 10, pp. 1–12, 2020.

[4] M. K. Mostafa, A. S. Mahmoud, R. A. Saryel-Deen, and R. W. Peters, "Application of entrapped nano zero valent iron into cellulose acetate membranes for domestic wastewater treatment," in *Environmental aspects, applications and implications of nanomaterials and nanotechnology 2017–Topical conference at the 2017 AIChE annual meeting* 27–34, Minneapolis, MN, United States, 2017.

[5] Z. Othman, H. R. Mackey, and K. A. Mahmoud, "A critical overview of MXenes adsorption behavior toward heavy metals," *Chemosphere*, vol. 295, p. 133849, 2022.

[6] R. A. Saryel-Deen, A. S. Mahmoud, M. Mahmoud, M. K. Mostafa, and R. W. Peters, "Adsorption and kinetic studies of using entrapped sewage sludge ash in the removal of chemical oxygen demand from domestic wastewater, with artificial intelligence approach," *AIChE Annual Meeting*, vol. 3, pp. 1587–1594, 2017.

[7] M. Nasr, "Modeling applications in environmental bioremediation studies," in *Phytobiont and Ecosystem Restitution*, pp. 143–160, Springer, Singapore, 2018.

[8] Z. Iqbal, M. S. Tanweer, and M. Alam, "Recent advances in adsorptive removal of wastewater pollutants by chemically modified metal oxides: a review," *Journal of Water Process Engineering*, vol. 46, p. 102641, 2022.

[9] M. Nasr, "Modeling applications in bioremediation of hydrocarbon pollutants," in *Microbial Action on Hydrocarbons*, pp. 181–197, Springer, Singapore, 2018.

[10] A. S. Mahmoud, R. A. Saryel-Deen, M. K. Mostafa, and R. W. Peters, "Artificial intelligence for organochlorine pesticides removal from aqueous solutions using entrapped nzvi in alginate biopolymer," in *Annual AIChE Meeting. Minneapolis*, pp. 420–427, Minneapolis, MN, United States, October 2017.

[11] A. S. Mahmoud, R. S. Farag, M. M. Elshfai, L. A. Mohamed, and S. M. Ragheb, "Nano zero-valent aluminum (nZVAl) preparation, characterization, and application for the removal of soluble organic matter with artificial intelligence, isotherm study, and kinetic analysis," *Air, Soil and Water Research*, vol. 12, p. 117862211987870, 2019.

[12] G. Wang, Q. S. Jia, M. Zhou, J. Bi, J. Qiao, and A. Abusorrah, "Artificial neural networks for water quality soft-sensing in wastewater treatment: a review," *Artificial Intelligence Review*, vol. 55, no. 1, pp. 565–587, 2022.

[13] A. S. Mahmoud, M. K. Mostafa, and M. Nasr, "Regression model, artificial intelligence, and cost estimation for phosphate adsorption using encapsulated nanoscale zero-valent iron," *Separation Science and Technology (Philadelphia)*, vol. 54, no. 1, pp. 13–26, 2019.

[14] A. Hamdy, M. K. Mostafa, and M. Nasr, "Regression analysis and artificial intelligence for removal of methylene blue from aqueous solutions using nanoscale zero-valent iron," *International Journal of Environmental Science and Technology*, vol. 16, no. 1, pp. 357–372, 2019.

[15] M. Fawzy, M. Nasr, S. Adel, and S. Helmi, "Regression model, artificial neural network, and cost estimation for biosorption of Ni(II)-ions from aqueous solutions by Potamogeton pectinatus," *International Journal of Phytoremediation*, vol. 20, no. 4, pp. 321–329, 2018.

[16] M. Fawzy, M. Nasr, H. Nagy, and S. Helmi, "Artificial intelligence and regression analysis for Cd(II) ion biosorption from aqueous solution by Gossypium barbadense waste,"

Environmental Science and Pollution Research, vol. 25, no. 6, pp. 5875–5888, 2018.

[17] P. J. D. P. van de Witte, P. J. Dijkstra, J. W. A. Van den Berg, and J. Feijen, "Phase separation processes in polymer solutions in relation to membrane formation," *Journal of Membrane Science*, vol. 117, no. 1-2, pp. 1–31, 1996.

[18] M. El-Shafei, A. Mahmoud, M. Mostafa, and R. Peters, "Effects of entrapped nZVI in alginate polymer on BTEX removal," in *AIChE Annual Meeting*, pp. 15–22, San Francisco, CA, 2016.

[19] M. S. Mahmoud, M. K. Mostafa, S. A. Mohamed, N. A. Sobhy, and M. Nasr, "Bioremediation of red azo dye from aqueous solutions by _A_ spergillus niger strain isolated from textile wastewater," *Journal of Environmental Chemical Engineering*, vol. 5, no. 1, pp. 547–554, 2017.

[20] A. S. Mahmoud, M. K. Mostafa, and S. A. Abdel-Gawad, "Artificial intelligence for the removal of benzene, toluene, ethyl benzene and xylene (BTEX) from aqueous solutions using iron nanoparticles," *Water Supply*, vol. 18, no. 5, pp. 1650–1663, 2018.

[21] W. E. F. Apha Awwa, *Standard Methods for Examinations of Water and Wastewater*, Apha Wef Awwa, Washington, DC,, 21st ed edition, 2005.

[22] M. H. Beale, M. T. Hagan, and H. B. Demuth, *Neural Network Toolbox User Guide*, The Math Works Inc, Natick, 2004.

[23] O. I. Abiodun, A. Jantan, A. E. Omolara, K. V. Dada, N. A. Mohamed, and H. Arshad, "State-of-the-art in artificial neural network applications: a survey," *Heliyon*, vol. 4, no. 11, p. e00938, 2018.

[24] O. Axelsson, "A generalized conjugate gradient, least square method," *Numerische Mathematik*, vol. 51, pp. 209–227, 1987.

[25] I. Helland, "On the interpretation and use of R2 in regression analysis," *Biometrics*, vol. 43, no. 1, pp. 61–69, 1987.

[26] T. Kim, "T test as a parametric statistic," *Korean Journal of Anesthesiology*, vol. 68, no. 6, pp. 540–546, 2015.

[27] A. Hamdy, M. K. Mostafa, and M. Nasr, "Techno-economic estimation of electroplating wastewater treatment using zero-valent iron nanoparticles: batch optimization, continuous feed, and scaling up studies," *Environmental Science and Pollution Research*, vol. 26, no. 24, pp. 25372–25385, 2019.

[28] Y. H. Shih, C. Y. Hsu, and Y. F. Su, "Reduction of hexachlorobenzene by nanoscale zero-valent iron: kinetics, pH effect, and degradation mechanism," *Separation and Purification Technology*, vol. 76, no. 3, pp. 268–274, 2011.

[29] A. Ishag, Y. Li, N. Zhang et al., "Environmental application of emerging zero-valent iron-based materials on removal of radionuclides from the wastewater: a review," *Environmental Research*, vol. 188, p. 109855, 2020.

[30] M. Stefaniuk, P. Oleszczuk, and Y. S. Ok, "Review on nano zerovalent iron (nZVI): from synthesis to environmental applications," *Chemical Engineering Journal*, vol. 287, pp. 618–632, 2016.

[31] Q. Li, Z. Chen, H. Wang et al., "Removal of organic compounds by nanoscale zero-valent iron and its composites," *Science of the Total Environment*, vol. 792, p. 148546, 2021.

[32] F. M. Omar, H. A. Aziz, and S. Stoll, "Aggregation and disaggregation of ZnO nanoparticles: influence of pH and adsorption of Suwannee River humic acid," *The Science of the Total Environment*, vol. 468, pp. 195–201, 2014.

[33] S. Bae and K. Hanna, "Reactivity of nanoscale zero-valent iron in unbuffered systems: effect of pH and Fe (II) dissolution," *Environmental science & technology*, vol. 49, no. 17, pp. 10536–10543, 2015.

[34] Y. Zhao, F. Liu, and X. Qin, "Adsorption of diclofenac onto goethite: adsorption kinetics and effects of pH," *Chemosphere*, vol. 180, pp. 373–378, 2017.

[35] R. Devi and R. P. Dahiya, "COD and BOD removal from domestic wastewater generated in decentralised sectors," *Bioresource Technology*, vol. 99, no. 2, pp. 344–349, 2008.

[36] S. Laohaprapanon, M. Marques, and W. Hogland, "Removal of organic pollutants from wastewater using wood fly ash as a low-cost sorbent," *Clean - Soil, Air, Water*, vol. 38, no. 11, pp. 1055–1061, 2010.

[37] A. S. Mahmoud, R. S. Farag, and M. M. Elshfai, "Reduction of organic matter from municipal wastewater at low cost using green synthesis nano iron extracted from black tea: artificial intelligence with regression analysis," *Egyptian Journal of Petroleum*, vol. 29, no. 1, pp. 9–20, 2020.

[38] M. A. Fulazzaky, M. H. Khamidun, and R. Omar, "Understanding of mass transfer resistance for the adsorption of solute onto porous material from the modified mass transfer factor models," *Chemical Engineering Journal*, vol. 228, pp. 1023–1029, 2013.

[39] A. E. A. Nayl, R. A. Elkhashab, T. El Malah et al., "Adsorption studies on the removal of COD and BOD from treated sewage using activated carbon prepared from date palm waste," *Environmental Science and Pollution Research*, vol. 24, no. 28, pp. 22284–22293, 2017.

[40] I. Langmuir, "The constitution and fundamental properties of solids and LIQUIDS. PART I. SOLIDS," *Journal of the American Chemical Society*, vol. 38, no. 11, pp. 2221–2295, 1916.

[41] H. Freundlich, "Over the adsorption in solution," *Journal of Physical Chemistry*, vol. 57, pp. 385–471, 1906.

[42] M. I. Tempkin and V. J. A. P. C. Pyzhev, "Kinetics of ammonia synthesis on promoted iron catalyst," *Acta Physicochim USSR*, vol. 12, pp. 327–356, 1940.

[43] B. Boulinguiez, P. Le Cloirec, and D. Wolbert, "Revisiting the determination of Langmuir parameters application to tetrahydrothiophene adsorption onto activated carbon," *Langmuir*, vol. 24, no. 13, pp. 6420–6424, 2008.

[44] K. Y. Foo and B. H. Hameed, "Insights into the modeling of adsorption isotherm systems," *Chemical Engineering Journal*, vol. 156, no. 1, pp. 2–10, 2010.

[45] Y.-S. Ho, "Second-order kinetic model for the sorption of cadmium onto tree fern: a comparison of linear and non-linear methods," *Water Research*, vol. 40, no. 1, pp. 119–125, 2006.

[46] M. S. Hossain, F. Omar, A. J. Asis, R. T. Bachmann, M. Z. I. Sarker, and M. O. Ab Kadir, "Effective treatment of palm oil mill effluent using $FeSO_4.7H_2O$ waste from titanium oxide industry: Coagulation adsorption isotherm and kinetics studies," *Journal of Cleaner Production*, vol. 219, pp. 86–98, 2019.

[47] M. H. Bakr, M. Nasr, M. Ashmawy, and A. Tawfik, "Predictive performance of auto-aerated immobilized biomass reactor treating anaerobic effluent of cardboard wastewater enriched with bronopol (2-bromo-2-nitropropan-1,3-diol) via artificial neural network," *Environmental Technology and Innovation*, vol. 21, p. 101327, 2021.

[48] F. A. Ansari, M. Nasr, I. Rawat, and F. Bux, "Artificial neural network and techno-economic estimation with algae-based tertiary wastewater treatment," *Journal of Water Process Engineering*, vol. 40, p. 101761, 2021.